Received: 11 January 2022 | Revised: 1 August 2022 | Accepted: 8 August 2022

DOI: 10.1002/hipo.23468

RESEARCH ARTICLE

WILEY

Learning-related changes in cellular activity within mouse dentate gyrus during trace eyeblink conditioning

Lisa N. Miller | Craig Weiss | John F. Disterhoft

Department of Neuroscience, Feinberg School of Medicine, Northwestern University, Chicago, Illinois, USA

Correspondence
Lisa N. Miller, Department of Neuroscience, Feinberg School of Medicine, Northwestern University, Chicago, IL 60611, USA.
Email: lisamiller2021@u.northwestern.edu

Funding information
National Institute on Aging, Grant/Award Numbers: R37 AG008796, RF1 AG017139; National Institutes of Health

[Correction added on September 01, 2022, after first online publication: Orcid id was updated for Craig Weiss.]

Abstract

Because the dentate gyrus serves as the first site for information processing in the hippocampal trisynaptic circuit, it an important structure for the formation of associative memories. Previous findings in rabbit had recorded populations of cells within dentate gyrus that may bridge the temporal gap between stimuli to support memory formation during trace eyeblink conditioning, an associative learning task. However, this previous work was unable to identify the types of cells demonstrating this type of activity. To explore these changes further, we did in vivo single-neuron recording in conjunction with physiological determination of cell types to investigate the functional role of granule cells, mossy cells, and interneurons in dentate gyrus during learning. Tetrode recordings were performed in young-adult mice during training on trace eyeblink conditioning, a hippocampal-dependent temporal associative memory task. Conditioned mice were able to successfully learn the task, with male mice learning at a faster rate than female mice. In the conditioned group, granule cells tended to show an increase in firing rate during conditioned stimulus presentation while mossy cells showed a decrease in firing rate during the trace interval and the unconditioned stimulus. Interestingly, populations of interneurons demonstrated learning-related increases and decreases in activity that began at onset of the conditioned stimulus and persisted through the trace interval. The current study also found a significant increase in theta power during stimuli presentation in conditioned animals, and this change in theta decreased over time. Ultimately, these data suggest unique involvement of granule cells, mossy cells, and interneurons in dentate gyrus in the formation of a trace associative memory. This work expands our knowledge of dentate gyrus function, helping to discern how aging and disease might disrupt this process.

KEYWORDS
dentate gyrus, granule cell, interneuron, learning, mossy cell

1 | INTRODUCTION

As the first region within the classic hippocampal trisynaptic circuit, the dentate gyrus (DG) is an important region for the formation of associative memories. The most numerous neuron type within DG are granule cells (GCs), which are glutamatergic cells that make up the densely packed granule cell layer (Amaral et al., 1990). GCs are sparse-firing, and it is believed that these cells allow DG to perform

pattern separation, which produces distinct neural connections for unique memories (Neunuebel & Knierim, 2014; Yassa & Stark, 2011). Optogenetic inactivation of GCs, and DG as a whole, has demonstrated that the region is necessary to encode associative memories (Bernier et al., 2017; Kheirbek et al., 2013). However, DG contains another type of glutamatergic neuron, which are the large mossy cells (MCs) located in the hilus, between the two blades of the granule cell layer (Amaral, 1978). MCs and GCs have reciprocal connections to modulate each other's activity, through both direct excitatory and indirect inhibitory pathways (Jinde et al., 2013). While loss of MCs is a common characteristic of epilepsy and brain injury, selective ablation of MCs leads to impairment in a context discrimination task (Jinde et al., 2012), inhibition of MCs impairs learning, but not memory retrieval, on an object location task (Bui et al., 2018), and selective excitation of MCs impairs acquisition of contextual fear conditioning (Botterill et al., 2021). However, the functional role of MCs in associative learning has not been thoroughly examined. More broadly, the relative contributions of MCs and GCs to memory acquisition in tasks that directly require neither pattern separation, nor spatial navigation, remains to be explored.

The DG also contains multiple types of interneurons (INs), which receive input from GCs and MCs and are important for coordinating population activity within DG. Two of the major groups of INs within DG are parvalbumin-expressing INs (PVIs) and somatostatin-expressing INs (SOMIs). PVIs are fast-spiking and inhibit the axon-initial and perisomatic domains of GCs (Hainmueller & Bartos, 2020). Meanwhile, SOMIs inhibit distal dendrites of GCs, and some SOMIs send long-range axonal projections to regions such as CA3, CA1, and subiculum, which may support information processing in neighboring hippocampal areas (Buckmaster et al., 2002; Hainmueller & Bartos, 2020; Yuan et al., 2017). DG INs are vital for regular functioning; for example, ablation of PVIs in ventral, but not dorsal, DG produces depression-like behaviors in mice (Chen et al., 2021). Additionally, inhibition of hilar GABAergic INs in dorsal DG impairs spatial learning and memory in the Morris Water Maze task (Andrews-Zwilling et al., 2012). However, the contributions of DG INs to the formation of trace associative memories remain to be investigated.

Learning-related changes in DG were observed by Berger et al. (1976) through use of multi-unit recordings in rabbits during delay eyeblink conditioning. In this study, Berger et al. (1976) observed an increase in cellular activity within DG very early in training that mimicked the behavioral response and preceded the behavioral activity in time. Suter et al. (2018) built upon this work by performing single-unit recordings from DG in rabbits during training on trace eyeblink conditioning (tEBC). Two populations of DG cells were observed that showed either an increase or decrease in firing rate that began at onset of the conditioned stimulus (CS), and this change in activity persisted through the trace interval until presentation of the unconditioned stimulus (US) (Suter et al., 2018). These data suggest a unique role for DG in an associative learning task that does not directly involve pattern separation. Specifically, these findings indicate that there may be DG cells demonstrating persistent firing in vivo, which would play an important role in memory formation by bridging the temporal gap between stimuli. However, this work had several limitations. Specifically, the identity of the types of DG cells making up these populations was unknown, as histology alone is not sufficient to determine what cell types were being recorded (GoodSmith et al., 2017; Senzai & Buzsáki, 2017). Additionally, most of the rate changes observed in Suter et al. (2018) were driven by cells with baseline firing rates of >2 Hz, which is greater than the average baseline firing rates of GCs and MCs and suggests that the majority of these cells were INs (GoodSmith et al., 2017; Senzai & Buzsáki, 2017).

To build upon these previous findings, the current study makes use of single-unit recording from DG in mice during training on tEBC, a hippocampal-dependent temporal associative memory task. During tEBC, an otherwise neutral CS is paired with an aversive US that causes a reflexive eyeblink response, and the two stimuli are separated in time by a stimulus-free trace interval. After repeated paired presentations of stimuli, the animal will start to close its eye prior to US onset, which is known as the conditioned response (CR). It takes many trials for mice to fully learn this task, which allows us to compare the rate of learning between different groups and to investigate the changes in cellular activity relative to behavioral expression of learning. Ultimately, we utilized the known physiological differences between DG cell types (GoodSmith et al., 2017; Senzai & Buzsáki, 2017) to determine what changes in activity were occurring in which cell types during this behavioral task.

The goal of this study was to determine the learning-related changes in activity of GCs, MCs, and INs in DG, using both male and female mice. Ultimately, we found that GCs tended to show a learning-related increase in firing rate during CS presentation while MCs showed a learning-related decrease in activity during the trace and US intervals. Interestingly, large learning-related increases and decreases in activity were observed in populations of INs that spanned the trace interval. These data suggest unique involvement of GCs, MCs, and INs in DG in the formation of a trace associative memory.

2 | MATERIALS AND METHODS

2.1 | Animals

Animal care procedures were conducted in accordance with NIH guidelines and as approved by the Northwestern University Institutional Animal Care and Use Committee. C57BL/6J mice were obtained from Jackson Labs (Stock # 000664) and housed in a Northwestern University animal facility on a 14/10 light–dark cycle with ad libitum access to food and water. Both male and female mice were used in this study, and estrous cycle was not monitored, as previous work has shown that difference in estrous cycle phase does not cause greater variability in female mice (Fritz et al., 2017; Prendergast et al., 2014). Animals were group-housed upon arrival and given at least a week to acclimate to the facility before undergoing microdrive implantation surgery. Following surgery all animals were housed individually in cages without a wire-top to prevent damage to the microdrive implant. Animals were approximately 10–14 weeks old at the beginning of behavioral training. Figure 1a depicts the complete experimental timeline.

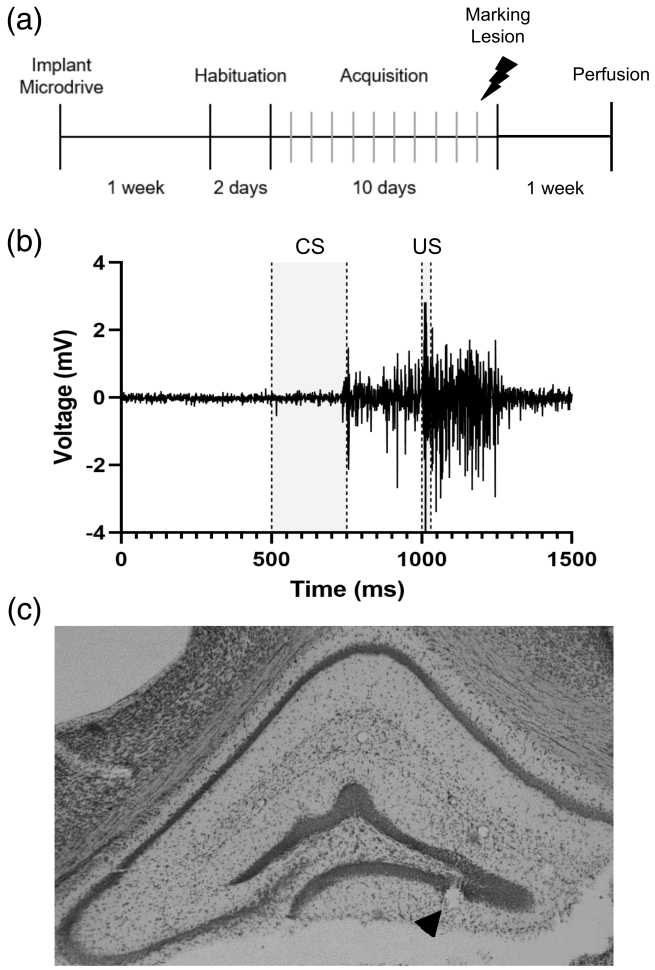

FIGURE 1 Experimental design and histology. (a) Experimental timeline for single-unit recording during tEBC. (b) Example of a raw EMG trace from a mouse in the conditioned group, showing a well-timed CR. Presentation of the CS and US are depicted by the gray bars. (c) Sample histology, showing the recording site of a tetrode in the lower blade of DG (black arrow). CR, conditioned response; CS, conditioned stimulus; DG, dentate gyrus; tEBC, trace eyeblink conditioning; US, unconditioned stimulus

2.2 | Microdrive implantation

For in vivo single-unit recording, we used the Neuralynx Halo-10-Mini microdrive, which can support up to eight independently movable tetrodes. The microdrives were assembled according to the manufacturer's instructions. Tetrodes were made from tungsten wire (California Fine Wire Co., Stock # CFW0011845) using the Neuralynx Tetrode Assembly Station, and were not plated. Before implantation, the impedance of each tetrode was tested in PBS using the nanoZ system to confirm that wires were not shorted (<150 kΩ), and rinsed with 70% ethanol before implantation.

To implant the microdrive, mice were kept in a surgical plane of anesthesia with isoflurane. A craniotomy, approximately 2.5 mm in diameter, was created centered at AP: −2.0 mm, ML: +1.5 mm. The microdrive ground wire was wrapped around a stainless-steel screw implanted in the skull above the cerebellum, and the microdrive was positioned over the craniotomy with the tetrode tips touching the surface of the brain. A layer of silicone grease (Danco) was applied surrounding the space between the exit tip and craniotomy to prevent adhesive from touching the tetrodes. The microdrive was secured in place with Metabond adhesive (Parkell Inc.) and dental cement (Coltene Hygenic Repair Resin). After cementing the microdrive in place, subdermal wires were placed around the orbicularis oculi muscle to measure eyeblink response via EMG activity. The ground wire for the EMG was secured to a reference screw implanted in the skull anterior of the coronal suture. Finally, two 3D-printed head-fixation bars were cemented to the implant above the animal's ears. Upon successful recovery from anesthesia, mice were returned to their home cage.

2.3 | Electrophysiology

The day following the implantation surgery, mice were placed in the behavioral chamber and tetrodes were advanced daily (0.25–1 mm/day) for approximately a week until reaching DG, as based on turn count, firing characteristics, and local field potential (LFP) profile (Bragin et al., 1995; Chi et al., 2016; GoodSmith et al., 2017). Electrical signals recorded from the tetrodes were acquired using the Digital Lynx SX system and recorded with Cheetah Data Acquisition Software (Neuralynx, Inc.) for offline analysis with custom Python scripts. For each animal a tetrode located outside of DG with little to no activity was used as a reference. Signals were sampled continuously at 32 kHz, and filtered between 300 and 6000Hz for single units and between 1 and 400 Hz for local field potentials.

2.4 | Trace eyeblink conditioning

Following approximately a week of lowering tetrodes, the mice were habituated to the training chamber for 2 days, for about 40 min per day. If necessary, tetrodes were adjusted after completion of each habituation session. The animals then underwent a total of 10 days of training, during which the tetrodes were not adjusted. During tEBC, mice were head-fixed atop a freely rotating cylinder (Heiney et al., 2014; Lin et al., 2016).

Animals were divided into two groups: conditioned and pseudo-conditioned (pseudo). Mice in the conditioned group received 50 paired trials per session. Each paired trial consisted of a 250-ms tone (CS; 2 kHz at 70 dB) and a 30-ms puff of compressed nitrogen delivered by a blunted 16-gauge needle directed at the cornea (US; 7.2 ± 0.2 psi). The two stimuli were separated by a 250-ms stimulus-free trace interval, and the mean intertrial interval was 45 s (range of 30–60 s). Mice in the pseudo group received 100 trials per session; consisting of 50 CS-only and 50 US-only trials, presented in a semi-random order. The mean intertrial interval for the pseudo group was 22 s (range of 15–30 s). Air pressure and tone amplitude were calibrated each day prior to training using a manometer (Fisher Scientific) and a sound meter (RadioShack), respectively. Custom LabView

software was used to control stimuli presentation, data collection, and data analysis. CRs were defined as EMG activity during the 200-ms prior to US onset that was >4 standard deviations above baseline for >15-ms, with the baseline being defined as 250-ms prior to CS onset. An example of a well-timed CR is shown in Figure 1b. An animal was considered to reach learning criterion when it showed CRs for at least 60% of trials within a session.

2.5 | Histology

Immediately following the final training session, mice were briefly anesthetized with a ketamine-xylazine cocktail and current (12 μA for 8–12 s) was passed through tetrodes to create electrolytic lesions using the nanoZ device and software. One week after the marking lesions were made, the animals underwent an intracardial perfusion with 0.1 M phosphate buffered saline (PBS) followed by 4% paraformaldehyde (PFA). The head was removed, with the microdrive implant still in place, and stored in 4% PFA at 4°C. Approximately 72 h later the brains were removed, rinsed with PBS, and stored in 30% sucrose in PBS for cryoprotection. The brains were then sliced on a freezing microtome to create 40 μm horizontal sections. Sections were mounted onto Superfrost Plus slides (Fisherbrand), dried, stained with cresyl violet, and viewed under a bright-field microscope to confirm the placement of each tetrode. Only recording data from tetrodes that were confirmed to be in DG through histological localization have been included in the analysis and results, excluding one tetrode located at the border of hilus and CA3. A sample image depicting the recording site of a tetrode that was successfully located in DG is shown in Figure 1c.

2.6 | Data analysis

Statistical analyses for learning curves were done with StatView, using repeated measures ANOVA (rmANOVA) to compare learning curves between groups and unpaired *t*-tests to compare groups on each day of training, with a Bonferroni adjusted alpha level of 0.005 per test, to determine statistically significant differences between groups for each session.

Single units were isolated using MountainSort, an automated spike sorting software package (Chung et al., 2017). Single units were automatically separated based on the following parameters: firing rate >0.05 Hz, isolation threshold >0.95, noise overlap threshold <0.015, and peak signal-to-noise ratio threshold >1.5. Following isolation, the average waveforms and clusters were visualized using MountainView. Occasionally, manual adjustments were made by joining two or more overlapping clusters, as based on the waveforms across all four tetrode wires and cluster overlap during visualization of the PCA features. Each cell was then assigned an isolation score, from 1 (poor) to 5 (very good), based on its separation from other clusters as visualized through PCA features, and whether there was noise present in the waveforms. Cells with a score of less than 3 were excluded from further analysis. Cells from male and female mice were combined, as well as cells across all days of training.

Tetrode location was not used as a factor in determining cell types, due to the fact that MCs and INs can produce large amplitude spikes that can be recorded from outside the hilus (e.g., from a tetrode in the GC layer) (Henze & Buzsáki, 2007; Senzai & Buzsáki, 2017). Instead, based on the characterization of DG neuron types by previous studies (Senzai & Buzsáki, 2017), single units were initially classified based on their average spike width (taken at half the maximal spike amplitude) and burst index. To calculate burst index, the sum of the number of spikes in the 3–5 ms bins of the spike autocorrelogram were divided by the average number of spikes in the 200–300 ms bins. After plotting these two features, three clusters were manually defined, based on the separation of cell types in Senzai and Buzsáki (2017): putative excitatory neurons (ENs), wide-waveform interneurons (wINs), and narrow-waveform interneurons (nINs).

ENs were further differentiated into GCs and MCs by plotting their average baseline firing rate against the average spike width for cells with average baseline firing rates less than 3 Hz, as based on the average firing rates of MCs and GCs in vivo (GoodSmith et al., 2017; Neunuebel & Knierim, 2014; Senzai & Buzsáki, 2017). Two clusters were then produced using *k*-means clustering in MATLAB, and manually adjusted; the cluster with mean firing rates less than 0.8 Hz was considered putative GCs, and the cluster with firing rates greater than 0.8 Hz was considered putative MCs. The average spike widths, baseline firing rates, and burst indices were compared between GC, MC, wIN, and nIN using unpaired *t*-tests (GraphPad Prism). Twenty cells from the putative EN group had baseline firing rates greater than 3 Hz, and were excluded from further analyses due to the ambiguity of the identity of these cells with high burst indices and high firing rates. Most likely, this group is comprised of multiple cell types, such as IN outliers, immature neurons, and/or semilunar granule cells.

For each cell, a peristimulus time histogram and raster plot were generated. The average firing rate of each cell during the CS, trace, and US intervals was evaluated using the Mann–Whitney *U* test to determine statistically significant changes compared to its baseline firing rate. Cells were then classified as either rate-increasing or rate-decreasing, based on their change in activity during the CS, trace, and US periods. The percentage of cells that showed either kind of rate change (increase or decrease) was compared between conditioned and pseudo mice using Fisher's exact test (GraphPad Prism).

For each of the four cell types (GCs, MCs, wINs, and nINs) from conditioned animals, the activity of rate-increasing and rate-decreasing cells was averaged and plotted in a peristimulus time histogram relative to the average activity of cells from pseudoconditioned animals. To more accurately compare the responses between cells from conditioned and pseudo mice, the first 1 s of activity (trial start through trace) in the pseudo histograms consisted of the average activity from CS-only trials, while the remaining 0.5 s (US onset to trial end) depicts the average activity from US-only trials (Suter et al., 2018). Average activity was compared between cells from conditioned and pseudoconditioned animals using a rmANOVA, with four 250-ms time intervals as the repeated measures: baseline (250-ms before CS onset), CS presentation, the trace interval, and US

TABLE 1 Statistics table

	Description	Type of test	Sample size	Statistical data
Figure 2: comparison of conditioned and pseudoconditioned groups	Conditioned vs. pseudo habituation	rmANOVA	Cond: $n = 23$ Pseudo: $n = 10$	*Group*: $F = 0.27$ $p = .61$ *Interaction*: $F = 0.009$ $p = .92$
	Conditioned vs. pseudo training	rmANOVA	Cond: $n = 23$ Pseudo: $n = 10$	*Group*: $F = 16.61$ $p = .0003$ *Interaction*: $F = 2.55$ $p = .0079$
	Cond vs. pseudo training	Unpaired *t*-test	Cond: $n = 23$ Pseudo: $n = 10$	T1: $p = .17$ T2: $p = .0063$ T3: $p = .0007$ T4: $p = .0004$ T5: $p = .0048$ T6: $p = .046$ T7: $p = .0039$ T8: $p = .0002$ T9: $p = .0041$ T10: $p = .0003$
	Male vs. female; pseudo habituation	rmANOVA	Male: $n = 4$ Female: $n = 6$	*Group*: $F = 0.097$ $p = .76$ *Interaction*: $F = 0.035$ $p = .86$
	Male vs. female; pseudo training	rmANOVA	Male: $n = 4$ Female: $n = 6$	*Group*: $F = 2.50$ $p = .15$ *Interaction*: $F = 0.79$ $p = .63$
	Male vs. female; conditioned habituation	rmANOVA	Male: $n = 15$ Female: $n = 8$	*Group*: $F = 2.26$ $p = .15$ *Interaction*: $F = 1.87$ $p = .19$
	Male vs. female; conditioned training	rmANOVA	Male: $n = 15$ Female: $n = 8$	*Group*: $F = 0.99$ $p = .33$ *Interaction*: $F = 2.82$ $p = .0040$
	Male vs. female; conditioned training	Unpaired *t*-test	Male: $n = 15$ Female: $n = 8$	T1: $p = .043$ T2: $p = .0099$ T3: $p = .1337$ T4: $p = .024$ T5: $p = .36$ T6: $p = .63$ T7: $p = .88$ T8: $p = .61$ T9: $p = .72$ T10: $p = .97$
Figure 3: comparison of recording subgroups and all animals	All vs. units; male Cond	rmANOVA	All: $n = 15$ Units: $n = 4$	*Group*: $F = 0.033$ $p = .86$

TABLE 1 (Continued)

	Description	Type of test	Sample size	Statistical data
				Interaction: $F = 0.81$ $p = .61$
	All vs. units; female Cond	rmANOVA	All: $n = 8$ Units: $n = 5$	*Group*: $F = 0.45$ $p = .52$ *Interaction*: $F = 0.63$ $p = .77$
	All vs. units; pseudo	rmANOVA	All: $n = 10$ Units: $n = 5$	*Group*: $F = 0.03$ $p = .86$ *Interaction*: $F = 0.54$ $p = .84$
Figure 4: comparison of single unit properties	nIN vs. GC/MC/wIN; spike width	Unpaired *t*-test	nIN: $n = 20$ GC: $n = 23$ MC: $n = 31$ wIN: $n = 25$	GC: $p < .0001$ MC: $p < .0001$ wIN: $p < .0001$
	GC vs. MC; baseline firing rate	Unpaired *t*-test	GC: $n = 23$ MC: $n = 31$	$p < .0001$
	wIN vs. MC/nIN; baseline firing rate	Unpaired *t*-test	wIN: $n = 25$ MC: $n = 31$ nIN: $n = 20$	MC: $p = .0001$ nIN: $p = .14$
	Burst index comparisons	Unpaired *t*-test	GC: $n = 23$ MC: $n = 31$ wIN: $n = 25$ nIN: $n = 20$	GC vs. MC: $p = .0091$ MC vs. nIN: $p < .0001$ nIN vs. wIN: $p < .0001$
Figure 5: comparison of Percentage Responsive Cells	Cond vs. pseudo; GC	Fisher's exact test	Cond: $n = 13$ Pseudo: $n = 10$	CS: $p = .34$ Trace: $p = .49$ US: $p = .18$ Overall: $p = .67$
	Cond vs. pseudo; MC	Fisher's exact test	Cond: $n = 19$ Pseudo: $n = 12$	CS: $p = .20$ Trace: $p = .47$ US: $p = .025$ Overall: $p = .13$
	Cond vs. pseudo; wIN	Fisher's exact test	Cond: $n = 11$ Pseudo: $n = 14$	CS: $p = .0072$ Trace: $p = .0002$ US: $p = .41$ Overall: $p = .020$
	Cond vs. pseudo; nIN	Fisher's exact test	Cond: $n = 7$ Pseudo: $n = 13$	CS: $p = .10$ Trace: $p = .0072$ US: $p = .33$ Overall: $p = .052$
Figure 7: comparison of average cell activity	Cond vs. pseudo; GC rate-increasing	rmANOVA	Cond: $n = 3$ Pseudo: $n = 10$	*Group*: $F = 6.54$ $p = .027$ *Interaction*: $F = 3.52$ $p = .026$
	Cond vs. pseudo; GC rate-increasing	Mann–Whitney *U* test	Cond: $n = 3$ Pseudo: $n = 10$	Baseline: $p = .74$ CS: $p = .028$ Trace: $p = .063$ US: $p = .18$
	Cond vs. pseudo; GC rate-decreasing	rmANOVA	Cond: $n = 3$	*Group*:

(Continues)

TABLE 1 (Continued)

	Description	Type of test	Sample size	Statistical data
			Pseudo: $n = 10$	$F = 0.085$ $p = .78$ *Interaction*: $F = 0.43$ $p = .73$
	Cond vs. pseudo; MC rate-increasing	rmANOVA	Cond: $n = 2$ Pseudo: $n = 12$	*Group*: $F = 6.93$ $p = .022$ *Interaction*: $F = 3.42$ $p = .027$
	Cond vs. pseudo; MC rate-increasing	Mann–Whitney *U* test	Cond: $n = 2$ Pseudo: $n = 12$	Baseline: $p = .86$ CS: $p = .029$ Trace: $p = .14$ US: $p = .068$
	Cond vs. pseudo; MC rate-decreasing	rmANOVA	Cond: $n = 13$ Pseudo: $n = 12$	*Group*: $F = 3.52$ $p = .073$ *Interaction*: $F = 4.94$ $p = .0036$
	Cond vs. pseudo; MC rate-decreasing	Mann–Whitney *U* test	Cond: $n = 13$ Pseudo: $n = 12$	Baseline: $p = .79$ CS: $p = .11$ Trace: $p = .0083$ US: $p = .0071$
	Cond vs. pseudo; wIN rate-increasing	rmANOVA	Cond: $n = 9$ Pseudo: $n = 14$	*Group*: $F = 14.85$ $p = 0.0009$ *Interaction*: $F = 5.57$ $p = 0.0019$
	Cond vs. pseudo; wIN rate-increasing	Mann–Whitney *U* test	Cond: $n = 9$ Pseudo: $n = 14$	Baseline: $p = .10$ CS: $p = .0051$ Trace: $p = .0038$ US: $p = .0046$
	Cond vs. pseudo; wIN rate-decreasing	rmANOVA	Cond: $n = 2$ Pseudo: $n = 14$	*Group*: $F = 1.31$ $p = .27$ *Interaction*: $F = 2.95$ $p = .044$
	Cond vs. pseudo; wIN rate-decreasing	Mann–Whitney *U* test	Cond: $n = 2$ Pseudo: $n = 14$	Baseline: $p = .34$ CS: $p = .63$ Trace: $p = .096$ US: $p = .057$
	Cond vs. pseudo; nIN rate-increasing	rmANOVA	Cond: $n = 7$ Pseudo: $n = 13$	*Group*: $F = 0.050$ $p = .83$ *Interaction*: $F = 3.79$ $p = .015$
	Cond vs. pseudo; nIN rate-increasing	Mann–Whitney *U* test	Cond: $n = 7$ Pseudo: $n = 13$	Baseline: $p = .32$ CS: $p = .55$ Trace: $p = .66$ US: $p = .45$
Figure 9: theta power analysis	CS vs. baseline; Cond	rmANOVA	$n = 9$	*Group*: $F = 18.35$ $p = .0011$

TABLE 1 (Continued)

	Description	Type of test	Sample size	Statistical data
				Interaction: $F = 3.16$ $p = .022$
	CS vs. baseline; Cond	Paired *t*-tests	$n = 9$	C − 2: $p = .0019$ C − 1: $p = .0057$ C: $p = .0016$ C + 1: $p = .0003$ C + 2: $p = .0092$
	US vs. baseline; Cond	rmANOVA	$n = 9$	*Group*: $F = 5.40$ $p = .039$ *Interaction*: $F = 2.95$ $p = .029$
	US vs. baseline; Cond	Paired *t*-tests	$n = 9$	C − 2: $p = .047$ C − 1: $p = .056$ C: $p = .0047$ C + 1: $p = .044$ C + 2: $p = .0046$
	CS vs. baseline; pseudo	rmANOVA	$n = 5$	*Group*: $F = 3.28$ $p = .11$ *Interaction*: $F = 0.42$ $p = .92$
	US vs. baseline; pseudo	rmANOVA	$n = 5$	*Group*: $F = 21.15$ $p = .0018$ *Interaction*: $F = 1.88$ $p = .068$
	US vs. baseline; pseudo	Paired *t*-tests	$n = 5$	T1: $p = .047$ T2: $p = .040$ T3: $p = .031$ T4: $p = .033$ T5: $p = .038$ T6: $p = .087$ T7: $p = .045$ T8: $p = .032$ T9: $p = .044$ T10: $p = .047$

Abbreviations: Cond, conditioned; CS, conditioned stimulus; GC, granule cell; MC, mossy cell; nIN, narrow-waveform interneuron; pseudo, pseudoconditioned; rmANOVA, repeated measures ANOVA; US, unconditioned stimulus; wIN, wide-waveform interneuron.

interval (250-ms after US onset). If rmANOVA revealed a significant interaction between group and time, post-hoc Mann–Whitney *U* tests were done to test for significant differences during each of the four time periods. The above analyses were completed using StatView.

To investigate whether the data could be skewed by oversampling the same cells across multiple days of training, a subgroup analysis was completed by only including cells from 1 day of training from each tetrode. For each tetrode, only the day with the most cells was included. If multiple days had the same number of cells, a day was chosen at random. The percentage of cells that showed a significant change in activity during the CS, trace, and/or US intervals were compared between conditioned and pseudo mice.

To examine changes in theta activity over the course of training, LFP data was filtered to the theta band in mice (4–10 Hz) (Senzai & Buzsáki, 2017) and theta power was calculated. Each trial was normalized relative to baseline (500-ms prior to CS), and then the trials were averaged to produce the mean for each day of training. Finally, mean theta power was averaged across animals for each session, using data collected from one tetrode per animal (the tetrode with the largest theta amplitude). Data from male and female mice were combined, and theta power was analyzed relative to the day each animal reached learning criterion to account for differences in rate of learning. Repeated measures ANOVA tests were completed with StatView to compare the change in theta power across days during CS

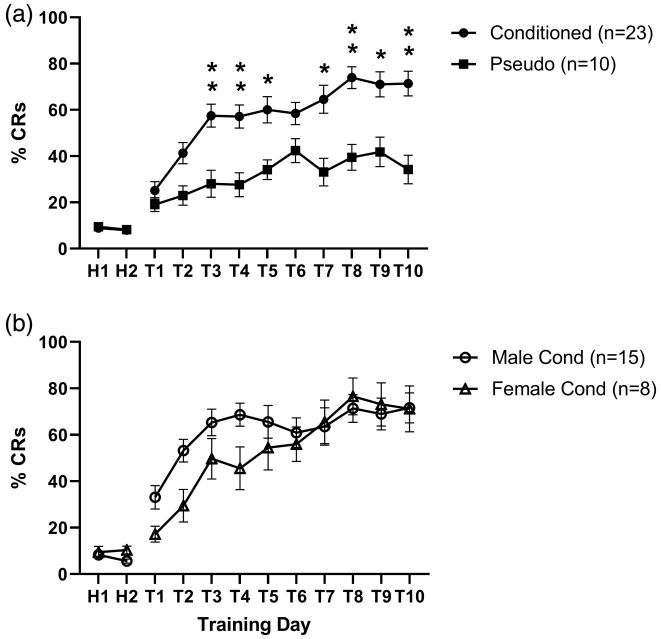

FIGURE 2 Trace eyeblink conditioning in microdrive mice. (a) Learning curves for all conditioned and pseudoconditioned animals. (b) Learning curves for conditioned animals, separated by sex. Average percent CRs are shown for each day, where "H" refers to days of habituation and "T" refers to days of training. Error bars represent *SEM*, and post-hoc unpaired *t*-tests were used to test statistical differences for each day of training, with a Bonferroni adjusted alpha level of 0.005 (* $p < .005$; ** $p < .001$). CR, conditioned response; DG, dentate gyrus

presentation, trace period, and US presentation, relative to baseline. Paired *t*-tests in MATLAB were used to test for significant differences on individual days. Days that had data from at least eight of nine animals were included for theta power analysis for conditioned animals; all days were included for pseudoconditioned mice.

Data are expressed as mean ± *SEM*, and, unless otherwise specified, $p < .05$ was considered statistically significant. A full list of statistical tests and results can be found in Table 1.

3 | RESULTS

3.1 | Behavioral results

Male and female mice implanted with microdrives to record from DG were trained for a total of 10 days on tEBC, receiving either paired (conditioned group, $n = 23$) or unpaired (pseudo group, $n = 10$) presentation of conditioned and unconditioned stimuli. EMG activity was used to quantify the animals' behavioral responses, and an animal was considered to have reached learning criterion when it showed CRs for at least 60% of trials within any session. The conditioned group received 50 paired trials per day and reached criterion on day 5 of training ("T5"), on average, while the pseudo group received 100 trials of unpaired stimuli per day and did not reach criterion (Figure 2a). There was no significant difference in performance (i.e. % CRs) during habituation ($F[1, 31] = 0.265$, $p = .61$), but there was a significant difference in performance between the conditioned and pseudo groups during training ($F[1, 31] = 16.61$, $p = .0003$), as well as a significant interaction between group and training day ($F[9, 279] = 2.55$, $p = .0079$). Unpaired t-tests revealed a significant difference between the two groups that started on the third day of training ("T3") ($p = .0007$) and continued until the final day of training ($p = .0003$). A complete list of *p*-values can be found in Table 1.

There was no significant difference between male and female mice in the pseudo group during either habituation ($F[1, 8] = 0.097$, $p = .76$) or training ($F[1, 8] = 2.49$, $p = .15$). While there was no overall significant difference between male and female conditioned mice during habituation ($F[1, 21] = 2.26$, $p = .15$) and training ($F[1, 21] = 0.99$, $p = .33$), there was a significant interaction of sex and day of training ($F[9, 189] = 2.82$, $p = .0040$), as male mice learned faster than the females. On average, male mice reached criterion on day 3 of training ("T3") while female mice reached criterion on day 7 ("T7") (Figure 2b). After correcting for multiple comparisons, however, unpaired t-tests showed no significant difference between male and female conditioned mice on any single training day.

After determining through histology which tetrodes were successfully located in DG, only a subset of animals were used for single-neuron and LFP analyses. There was no significant difference between the behavior of these subgroups of animals and the behavior of all animals, as shown in Figure 3 (male: $F[1, 17] = 0.033$, $p = .86$; female: $F[1, 11] = 0.447$, $p = .52$; pseudo: $F[1, 13] = 0.03$, $p = .86$).

3.2 | Differentiating neuron types

After confirming which tetrodes were located in DG through histology, single-unit data collected from a total of nine conditioned and five pseudoconditioned animals were analyzed. The average impedence of the tetrodes located in DG was 238.51 ± 9.27 kΩ. The full breakdown of the number of cells from each group and from each sex is shown in Table 2.

Initial classification of single units was done through plotting the burst index against spike width for each cell (Figure 4a). Manually, three clusters were determined; putative ENs had a high burst index, wINs had a low burst index, and nINs had narrow spike widths and intermediate burst indices. ENs were then further differentiated into putative GCs and MCs based on their spike widths and baseline firing rates (Figure 4b). Ultimately, nINs had significantly narrower spike widths than the other cell types, and there was no statistically significant difference in spike width between any of the other three cell types (Figure 4c). As well, GCs had significantly lower baseline firing rates than MCs, as expected based on the differentiation of these cells types by firing rate. Both types of INs had significantly higher firing rates than both GCs and MCs (Figure 4d). Finally, all four types of cells had significantly different burst indices, with GCs having the largest and wINs having the smallest burst index (Figure 4e). A summary

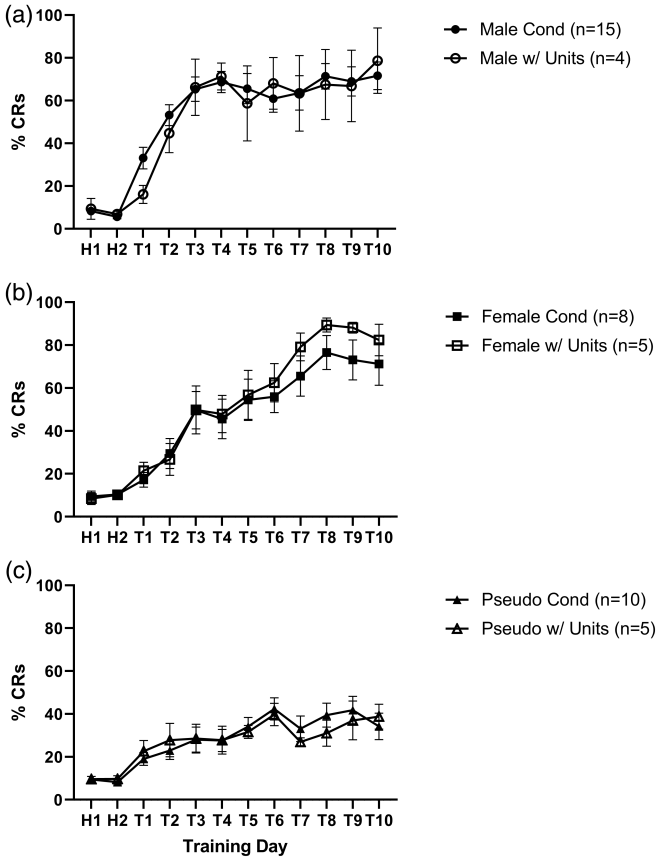

FIGURE 3 Recording data subgroup replicates overall behavior. Learning curves for male conditioned mice (a), female conditioned mice (b), and pseudoconditioned mice (c), comparing average percent CRs between all animals (filled symbols) and animals that had single units recorded from DG, as verified by histology (open symbols). "H" refers to days of habituation and "T" refers to days of training. Error bars represent *SEM*. CR, conditioned response; DG, dentate gyrus

of the properties and number of cells from each group is shown in Table 3.

3.3 | Single unit learning-related changes

All cells were classified as either rate-increasing or rate-decreasing based on whether they showed a significant change in firing rate during the CS, trace, or US intervals, relative to baseline. The percentage of cells that showed a significant rate change during one, or any ("Overall"), of these time periods are depicted in Figure 5. Ultimately, there was no significant difference between the percentage of GCs from conditioned and pseudoconditioned animals that showed significant changes in firing rates. However, a greater percentage of MCs from conditioned animals showed significant changes in activity relative to MCs from pseudo animals, specifically during the US interval ($p = .025$). Additionally, wINs from conditioned animals had a greater percentage of rate changing cells than wINs from pseudo animals ($p = .020$); specifically, more wINs from conditioned mice showed changes during the CS ($p = .0072$) and trace intervals ($p = .0002$). Finally, a greater percentage of nINs from conditioned animals showed significant changes in activity relative to nINs from pseudo animals during the trace interval ($p = .0072$).

TABLE 2 Summary of single-unit data composition

	Conditioned		Pseudoconditioned	
Number of animals	4 M	5 F	3 M	2 F
Total cells	81		58	
Cells from males/females	27/54		26/32	

Abbreviations: F, female; M, male.

To ensure that the data were not skewed by oversampling the same cells across multiple days of training, a subgroup of cells were selected by only examining cells from a single day for each tetrode (Figure 6a,b). The percentage of these cells that showed a significant rate change during one or any of the behavioral time periods are shown in Figure 6c. Ultimately, the results of the subgroup analysis mirror the results of the full dataset. Specifically, a greater percentage of MCs from conditioned animals showed significant changes in activity compared to MCs from pseudo animals, particularly during the US interval. Additionally, both wINs and nINs from conditioned mice showed a greater percentage of rate changing cells than INs from pseudo mice, particularly during the trace interval.

The activity patterns of rate-increasing and rate-decreasing cells from conditioned animals for each of the four cell types were averaged and compared to the average activity patterns of cells from pseudoconditioned animals to confirm that changes in activity were not simply due to stimulus presentation (Figure 7). To provide the most accurate comparison between groups, activity of cells from pseudo mice was plotted as a composite line, combining CS-only trials (0–1 s; trial start through trace interval) and US-only trials (1–1.5 s; US onset to trial end).

Ultimately, GCs from conditioned mice showed a significant increase in activity compared to GCs from pseudo mice (Group: $F[1, 11] = 6.54$, $p = .027$; Interaction: $F[3, 33] = 3.52$, $p = .026$), and this increase was statistically significant during CS presentation ($p = .028$) (Figure 7a). Rate-increasing MCs from conditioned mice also showed a significant increase in activity relative to MCs from pseudo mice (Group: $F[1, 12] = 6.93$, $p = .022$; Interaction: $F[3, 36] = 3.42$, $p = .027$) during CS presentation ($p = .029$). Rate-decreasing MCs from conditioned animals showed a significant decrease in activity relative to MCs from pseudoconditioned animals (Group: $F[1, 23] = 3.52$, $p = .073$; Interaction: $F[3, 69] = 4.94$, $p = .0036$), and this difference was statistically significant during the trace ($p = .0083$) and US ($p = .0071$) intervals (Figure 7b).

Both wINs (Group: $F[1, 21] = 14.85$, $p = .0009$; Interaction: $F[3, 63] = 5.57$, $p = .0019$) and nINs (Group: $F[1, 18] = 0.050$, $p = .8254$; Interaction: $F[3, 54] = 3.79$, $p = .015$) from conditioned animals showed significant increases in activity relative to INs from

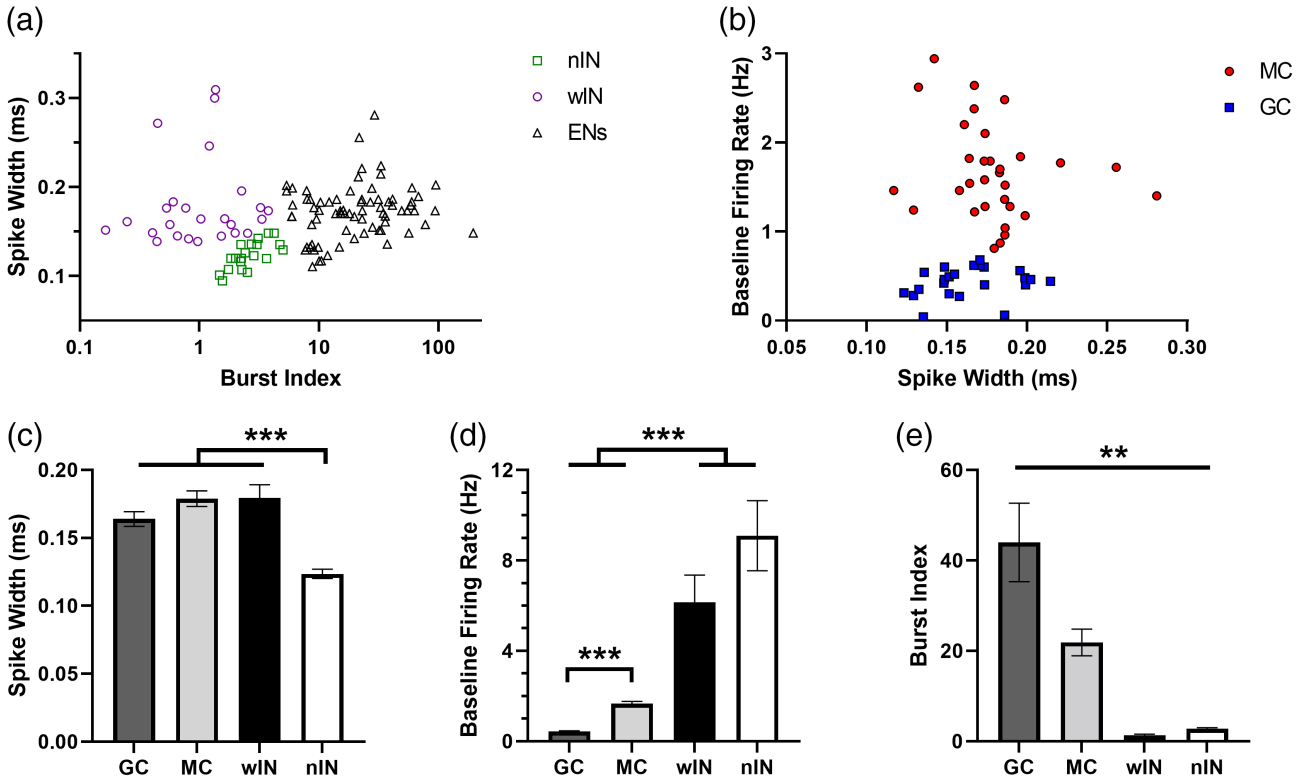

FIGURE 4 Firing properties of dentate gyrus cell types. (a) Plotting burst index against spike width for each cell yielded three clusters: putative excitatory neurons (EN; $n = 74$), narrow-waveform interneurons (nIN; $n = 20$), and wide-waveform interneurons (wIN; $n = 25$). (b) Excitatory neurons were further differentiated into mossy cells (MC; $n = 31$) and granule cells (GC; $n = 23$) by plotting their average baseline firing rate against spike width. (c) nINs have a significantly narrower average waveform than each of the three other cell types. (d) By definition, GCs have a significantly lower baseline firing rate than MCs. Both groups of interneurons have significantly higher baseline firing rates than GCs and MCs. (e) All four groups of cells had significantly different burst indices. Error bars represent *SEM* and unpaired *t*-tests were used to compare groups (* $p < .05$; *** $p < .001$)

TABLE 3 Summary of single-unit data by cell type

	GC	MC	wIN	nIN
Baseline firing rate (Hz)	0.43 ± 0.035	1.67 ± 0.097	6.16 ± 1.20	9.09 ± 1.55
Spike width (ms)	0.16 ± 0.0054	0.18 ± 0.0058	0.18 ± 0.0098	0.12 ± 0.0035
Burst index	43.99 ± 8.68	21.86 ± 2.95	1.35 ± 0.20	2.78 ± 0.23
Total cells	23	31	25	20
Cells from Cond/pseudo	13/10	19/12	11/14	7/13

Note: Data are presented as average ± *SEM*.
Abbreviations: Cond, conditioned; GC, granule cell; MC, mossy cell; nIN, narrow-waveform interneuron; pseudo, pseudoconditioned; wIN, wide-waveform interneuron.

pseudo mice. For wINs this increase was statistically significant during the CS ($p = .0051$), trace ($p = .0038$), and US intervals ($p = .0046$) (Figure 7c), while for nINs there was no statistically significant difference during any of the time intervals (Figure 7d). Rate-decreasing wINs from conditioned animals showed a significant decrease in activity, relative to activity in INs from pseudo mice (Group: $F[1, 14] = 1.31$, $p = .27$; Interaction: $F[3, 42] = 2.95$, $p = .044$), but there were no significant differences between any of the time intervals (Figure 7c).

Raster plots depicting activity of representative rate-increasing and rate-decreasing cells from each group are shown in Figure 8.

3.4 | Theta power

For conditioned animals, theta power was analyzed relative to the day that each animal reached criterion (day "C"), to account for different rates of learning. In the conditioned group ($n = 9$), theta power was significantly increased during CS ($F[1, 12] = 18.35$, $p = .0011$) and US ($F[1, 12] = 5.40$, $p = .039$) presentation, relative to baseline (Figure 9). There was also a significant interaction with day of training (CS: $F[4, 48] = 3.16$, $p = .022$; US: $F[4, 48] = 2.95$, $p = .029$), reflecting that these changes decreased from pre-criterion to post-criterion. Paired t-tests showed that the change in theta power during CS presentation

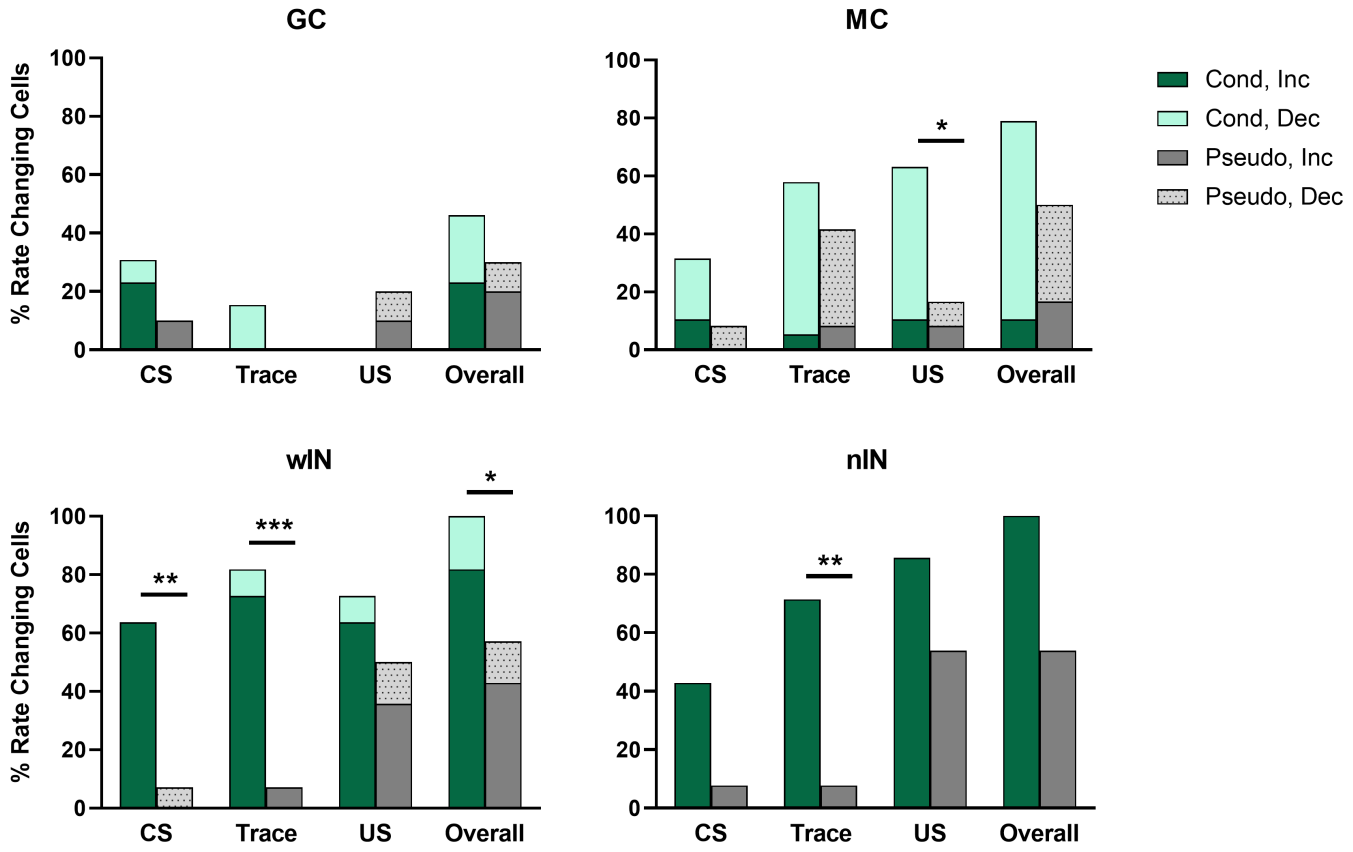

FIGURE 5 Percentage of significant rate-changing cells in conditioned and pseudoconditioned mice. Cells that showed a significant increase (dark green/dark gray) or decrease (light green/light gray) in firing rate during the CS, trace, or US interval, as determined by Mann–Whitney *U* test, are presented as a percentage of all cells within a group. Any cell that showed a significant change in firing rate during at least one of the three time periods was included in the "overall" count. Differences between groups were calculated using Fisher's exact test (* $p < .05$; ** $p < .01$; *** $p < .001$). CS, conditioned stimulus; US, unconditioned stimulus

was significant for all days. The change in theta power during US presentation was significant for every day except for the day before criterion ("C − 1"; $p = .056$). In pseudoconditioned animals ($n = 5$), there was no significant change in theta power during CS presentation, relative to baseline ($F[1, 8] = 3.28$, $p = .11$) (Figure 9). However, there was a significant increase in theta power during US presentation ($F[1, 8] = 21.15$, $p = .0018$), but there was no significant interaction with day of training ($F[9, 72] = 1.88$, $p = .068$), meaning that this change was consistent across days (Figure 9).

4 | DISCUSSION

This study used in vivo single-unit recording to investigate the changes in different DG cell types during associative learning. After histological confirmation of which tetrodes were located in DG, we utilized the known physiological differences between DG cell types to distinguish among MCs, GCs, wide-waveform INs, and narrow-waveform INs (GoodSmith et al., 2017; Neunuebel & Knierim, 2014; Senzai & Buzsáki, 2017). Ultimately these groups of neurons have similar firing properties as shown in previous work (GoodSmith et al., 2017; Neunuebel & Knierim, 2012; Senzai & Buzsáki, 2017), with GCs having a more narrow waveform and lower baseline firing rates than MCs, and INs having higher firing rates and lower burstiness than both GCs and MCs. In the current data, putative GCs have a significantly higher burst index than MCs which is in contrast to the data from GoodSmith et al. (2022). A likely reason for this difference is due to different approaches in calculating burst index/burstiness, and the fact that cells in GoodSmith et al. (2022) were classified based on their recording during sleep, while the current data classified cells during active behavior.

Rate-increasing GCs from conditioned mice showed a significant, and short latency, increase in activity during CS presentation while rate-decreasing MCs from conditioned mice showed a temporally-delayed, but significant decrease in firing rate during the trace and US intervals. Interestingly, wINs from conditioned mice showed a large increase in firing rate shortly after CS onset, and this increase in wIN activity persisted through the trace and US intervals. Finally, nINs from conditioned mice showed a significant increase in firing rate, relative to nINs from pseudoconditioned animals, but this change was not statistically significant during any particular time period.

Figure 10 demonstrates a hypothetical functional interpretation of the interactions of these changes in activity amongst the various cell types. Specifically, entorhinal cortex (EC) passes stimulus

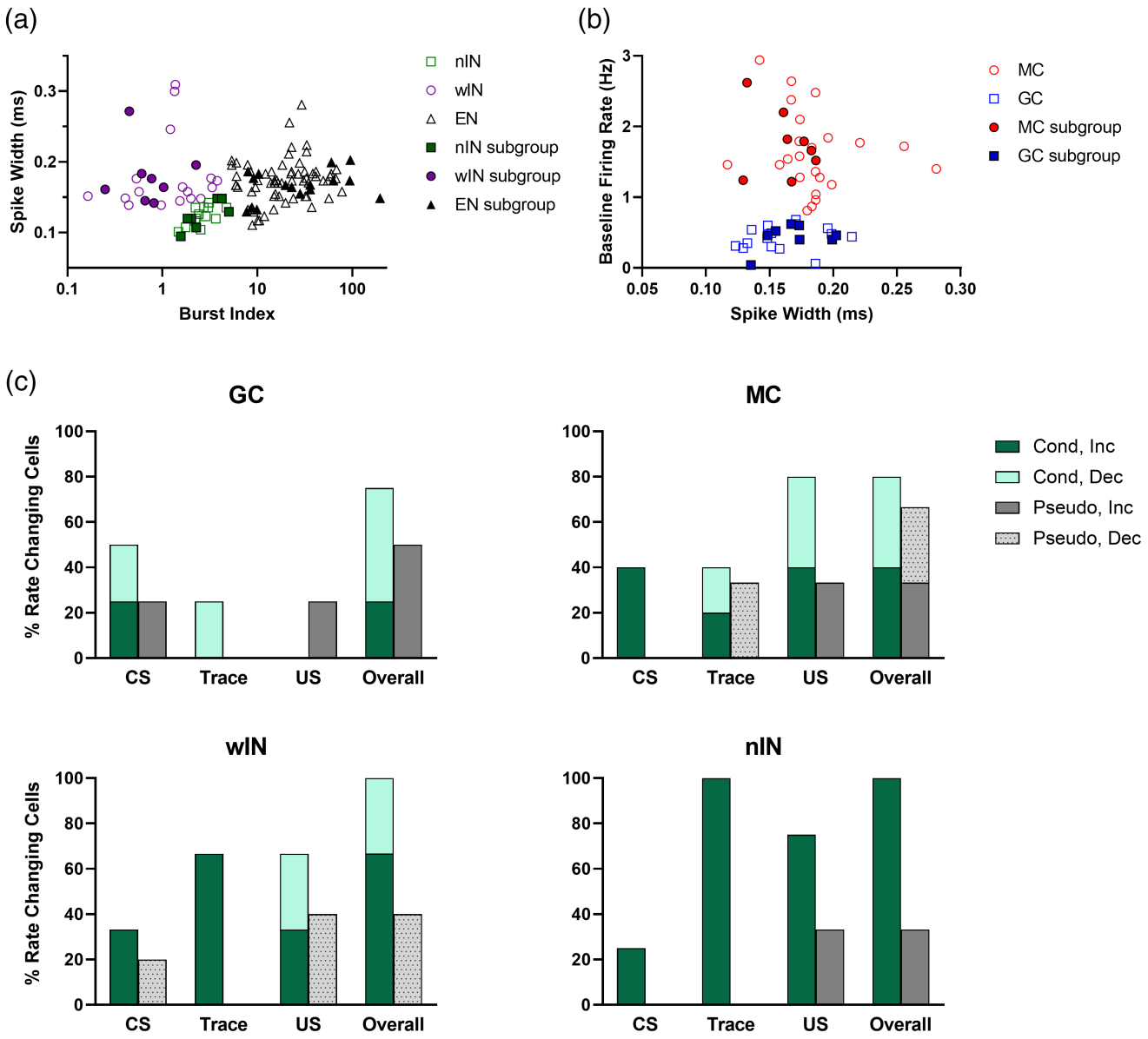

FIGURE 6 Subpopulation analysis shows similar trends as complete dataset. (a) Plot of burst index versus spike width for all cells shown in open symbols. A total of 8 wINs, 7 nINs, and 16 ENs (8 GCs, 8 MCs) were included in the subgroup analysis, depicted by the filled symbols. (b) Plot of average baseline firing rate versus spike width used to distinguish MCs and GCs; all data are shown by open symbols, and the cells used for the subgroup analysis are represented by filled symbols. (c) Percentage of significant rate-changing cells within the subgroups for each cell type. The number of cells from conditioned and pseudoconditioned animals, respectively, are as follows: GC: $N = 4$ and 4; MC: $N = 5$ and 3; wIN: $N = 3$ and 5; nIN: $N = 4$ and 3. EN, excitatory neuron; GC, granule cell; MC, mossy cell; nIN, narrow-waveform interneuron; wIN, wide-waveform interneuron

information on to GCs, which activates the increase in GC activity during CS onset (Figures 7a and 8a). GCs then project to INs, which coincides with the large increase in activity during the CS interval in both wINs and nINs (Figure 7c,d). While the nINs tend to mirror the activity patterns of rate-increasing GCs (Figure 8d), the wINs show a persistent increase in activity through the trace and US intervals (Figure 8c), which is likely due to repeated depolarizing inputs from GCs and increased excitability of the INs as a result of learning. It has been shown with biophysical approaches in brain slices in vitro that associative learning enhances intrinsic excitability of hippocampal INs in CA1 (McKay et al., 2013) and that DG INs, specifically parvalbumin-expressing perisoma-inhibiting INs, are capable of persistent firing (Elgueta et al., 2015). This persistent increase in activity of wINs likely then leads to the observed decrease in MC activity during the trace and US intervals (Figures 7b and 8b), due to the increased inhibitory input. This decrease in MC activity should have a net excitatory effect on GCs, promoting GC activity. Ultimately, GCs then send the processed information on to the CA3 region of the hippocampus.

These current data converge with and expand upon previous work done by Suter et al. (2018) that recorded from DG in rabbits

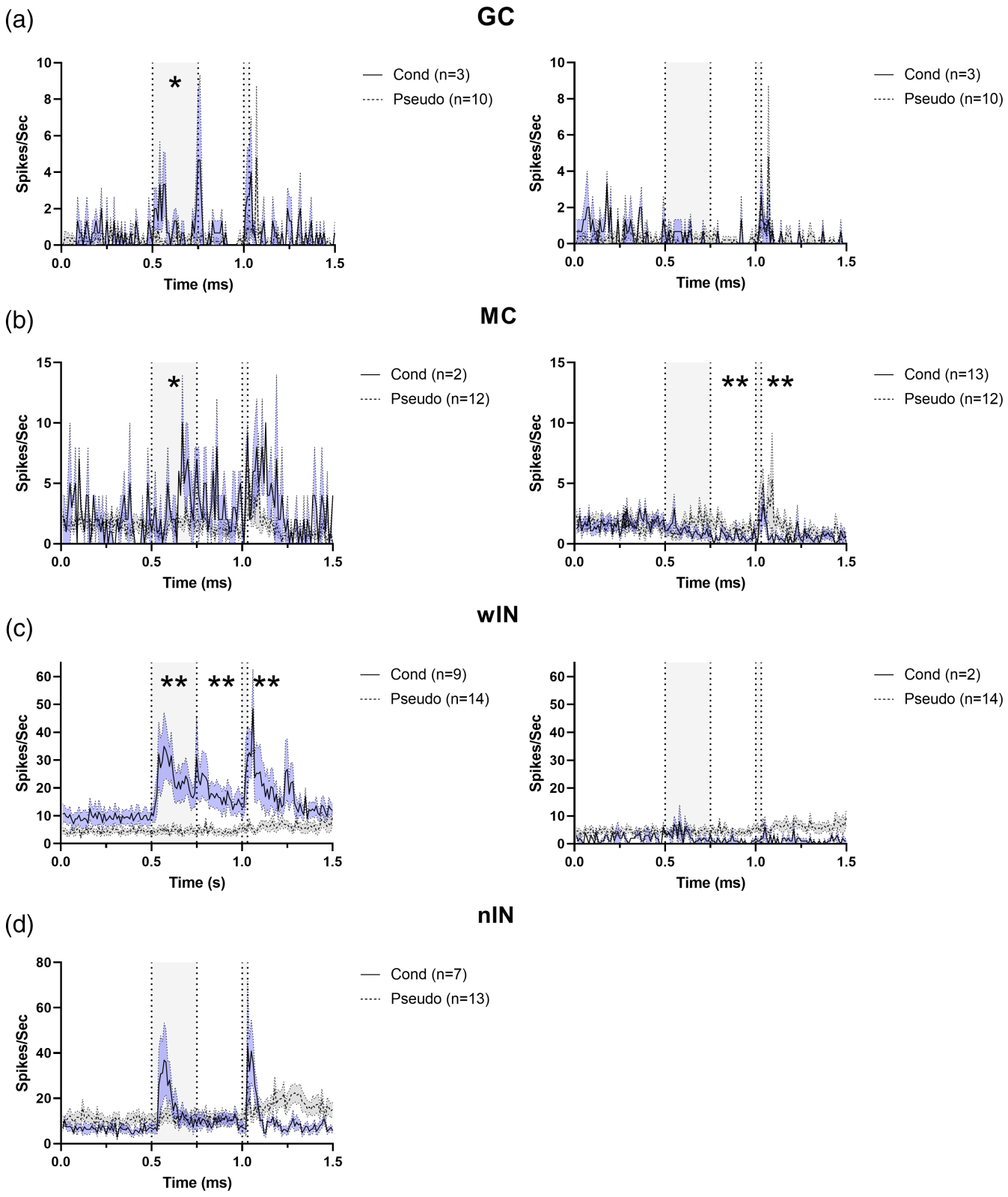

FIGURE 7 Learning-related changes in rate-increasing (left panels) and rate-decreasing cells (right panels). Peristimulus time histograms for GCs (a), MCs (b), wide-waveform INs (c), and narrow-waveform INs (d) depicting average activity from cells from conditioned animals (solid line) that displayed an increase (left) or decrease (right) in firing rate during the CS, trace, and/or US interval. Average activity of cells from pseudoconditioned animals (dashed line) are shown as a composite, combining CS-only trials (0–1 s) and US-only trials (1–1.5 s). Gray bars represent timing of CS and US presentation. Average activity across time was compared between cells from conditioned and pseudo mice using rmANOVA, and individual time periods were compared using post hoc Mann–Whitney *U* tests (* $p < .05$; ** $p < .01$). Shading represents *SEM*. CS, conditioned stimulus; GC, granule cell; IN, interneuron; MC, mossy cell; US, unconditioned stimulus

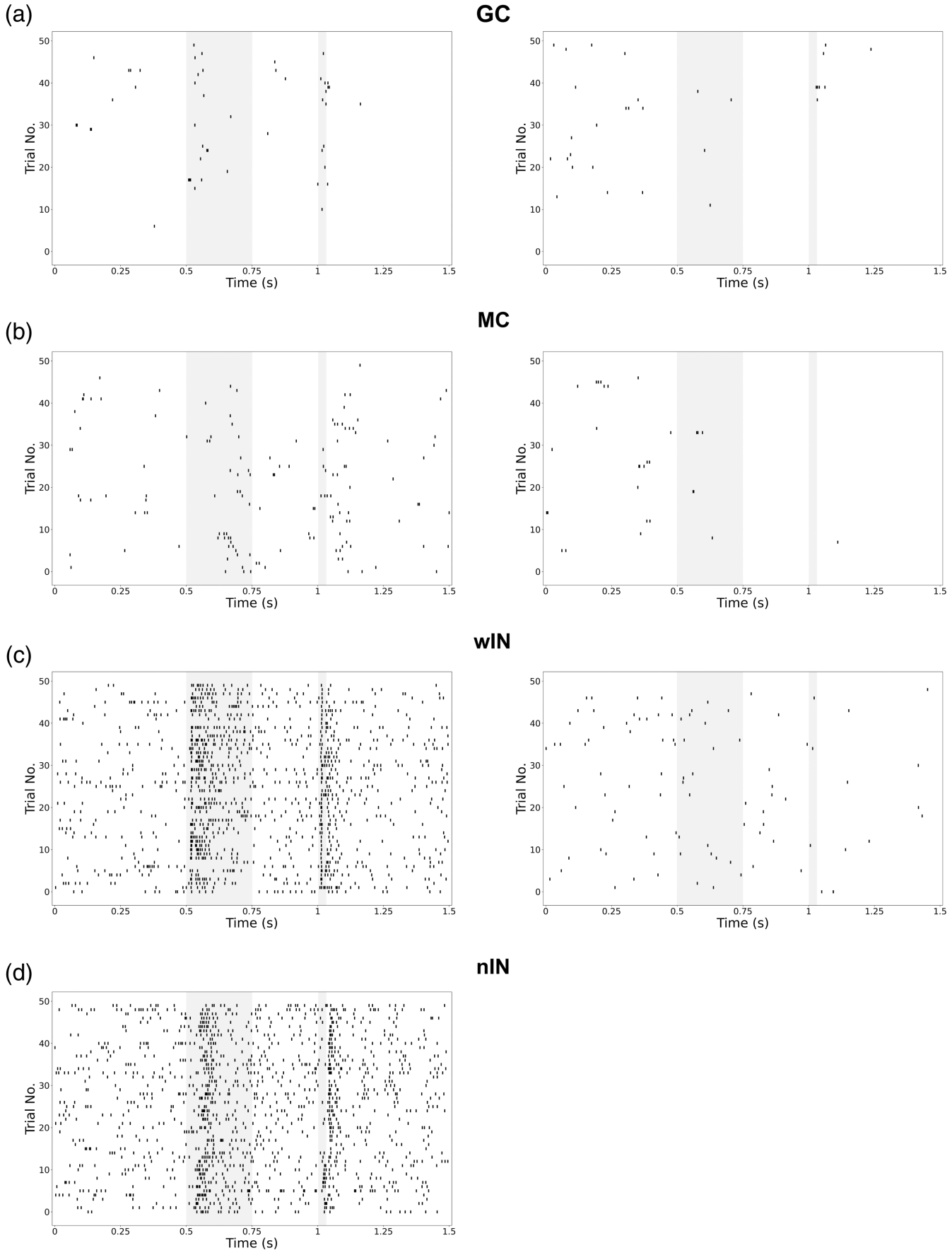

FIGURE 8 Legend on next page.

trained on tEBC. In Suter et al. (2018), there was a population of DG cells from conditioned animals that showed a large increase in firing rate during CS presentation, and this increase continued through the trace and US. These changes were largely driven by cells that had baseline firing rates between 2 and 10 Hz, and while these cells were hypothesized to be MCs or immature neurons (Suter et al., 2018), their activity closely aligns with the rate-increasing wINs from the current study. Suter et al. (2018) also observed a population of cells that showed a decrease in firing rate through the CS and trace intervals, which is similar to the activity patterns of rate-decreasing MCs and wINs in the current study. The limitation of Suter et al. (2018) was that they were unable to distinguish the cell types that displayed these activity patterns. Based on the physiological differences in DG cell types (GoodSmith et al., 2017; Neunuebel & Knierim, 2014; Senzai & Buzsáki, 2017), and the functional characteristics of the different neuron types in the current study, we can infer that a large portion of the DG cells presented in Suter et al. (2018) were INs.

It is interesting to consider the sequence of neuronal events shown in the average firing rate histograms of Figure 7 and the example raster plots of Figure 8 in relation to the functional diagram of the dentate gyrus indicated in Figure 10. The GCs show the earliest responses to input from the LEC perforant path as shown in the average neuronal firing histograms. GCs then project excitatory input: (1) to the mossy cells and (2) to the interneurons which in turn reciprocally inhibit the granule cells as well as the mossy cells for the remainder of the CS and through the trace interval. The IN inhibition causes the persistent MC reduction in firing that lasts through the trace interval. It will be interesting to further characterize these functional interactions with a combination of single neuron electrophysiology, cell type-specific excitation or inhibition driven optogenetically, and/or miniscope recording of calcium transients in large numbers of spatially contiguous neurons during and after learning of the trace eyeblink conditioned response. Such approaches will give us a more definitive description of the events occurring during the various portions of trials as learning occurs.

The current study also investigated changes in theta power in DG to determine how ensemble activity was affected by learning. We observed a significant increase in theta power during both CS and US presentations in conditioned mice, and this change decreased across days, from pre- to post-criterion. In the pseudo group, there was a large increase in theta power during US presentation, and this change was consistent across days. However, there was no significant change in theta power during CS presentation in the pseudo group. These results are similar to the data from Suter et al. (2018), who showed that in DG, theta power increased during CS and US presentation in conditioned rabbits, but decreased across days of training. Suter et al. (2018) also observed a large increase in theta power during US presentation in pseudoconditioned animals, as was shown in the current study. Interestingly, however, Suter et al. (2018) observed a significant increase in theta power during CS presentation in pseudo animals, while the current study found no significant change in theta power during CS-only trials. A reason for this difference could be due to the different stimuli used in each study. Suter et al. (2018) made use of a whisker vibration while the current study employed a tone as the CS. Because whisker stimulation is more biologically relevant to lagomorphs than a neutral tone, the information regarding a whisker vibration may be more likely to be passed on to the hippocampus than a tone, even when it is not learning-related.

Kitamura et al. (2015) showed that inhibiting ocean cells, which are medial EC cells that project to DG, during trace fear conditioning has no behavioral effect, while inhibiting island cells, which are medial EC cells that project directly to CA1, impairs temporal associative learning. These results suggest that the pathway from medial EC to DG is not necessary for trace learning, but other studies have shown that the DG is still involved in trace fear conditioning. Specifically, Gilmartin and McEchron (2005) observed a progressive increase in learning-related activity in DG neurons over time during trace fear conditioning, and Pierson et al. (2015) found that infusion of the AMPA/kainite receptor antagonist CNQX into DG, to inhibit the region, impaired expression of trace fear conditioned memories. Therefore, based on these past studies and the current study that shows clear learning-related changes within DG during tEBC, we hypothesize that it is the connection between lateral EC and DG that drives the involvement of DG in trace memory formation. The importance of lateral EC, and subsequently its downstream projections to DG, is supported by observed changes in lateral EC activity during tEBC (Suter et al., 2018) and the fact that inhibition of lateral EC during training impairs acquisition of differential tEBC (Yu et al., 2021).

Perhaps most striking is the large increase in activity in wINs from conditioned animals that spans the CS, trace, and US intervals. This increased inhibitory tone likely exerts its effect on both local and distant circuits, and could promote temporal bridging of information by inhibiting other INs. Within DG, this inhibition can serve to refine which GCs are activated by the incoming stimulus information, as both PVIs and SOMIs have been shown to regulate GC input transformations (Lee et al., 2016; Yuan et al., 2017), as well as help control the timing of GC activity (Royer et al., 2012; Savanthrapadian et al., 2014). Additionally, some SOMIs within DG project to other regions of the brain, including CA1, CA3, subiculum, and medial septum (Buckmaster et al., 2002; Yuan et al., 2017). Therefore, these external connections may also contribute to learning through inhibiting or refining activity of other brain regions. For example, in rabbits trained on delay eyeblink conditioning, cellular activity in medial septum only shows an increase during stimuli presentation (Berger & Thompson, 1978), which may be partially influenced by inhibition

FIGURE 8 Raster plots of representative cells from conditioned mice. (a) Example rate-increasing (left) and rate-decreasing (right) GCs, both recorded from day C. (b) Example rate-increasing (left) and rate-decreasing (right) MCs recorded from days C − 2 and C − 1, respectively. (c) Example rate-increasing (left) and rate-decreasing (right) wide-waveform INs recorded from days C + 8 and C-4, respectively. (d) Example rate-increasing narrow-waveform IN recorded from day C + 1. Gray bars represent CS and US presentation. Day "C" refers to the day that the animal reached learning criterion. GC, granule cell; IN, interneuron; MC, mossy cell; US, unconditioned stimulus

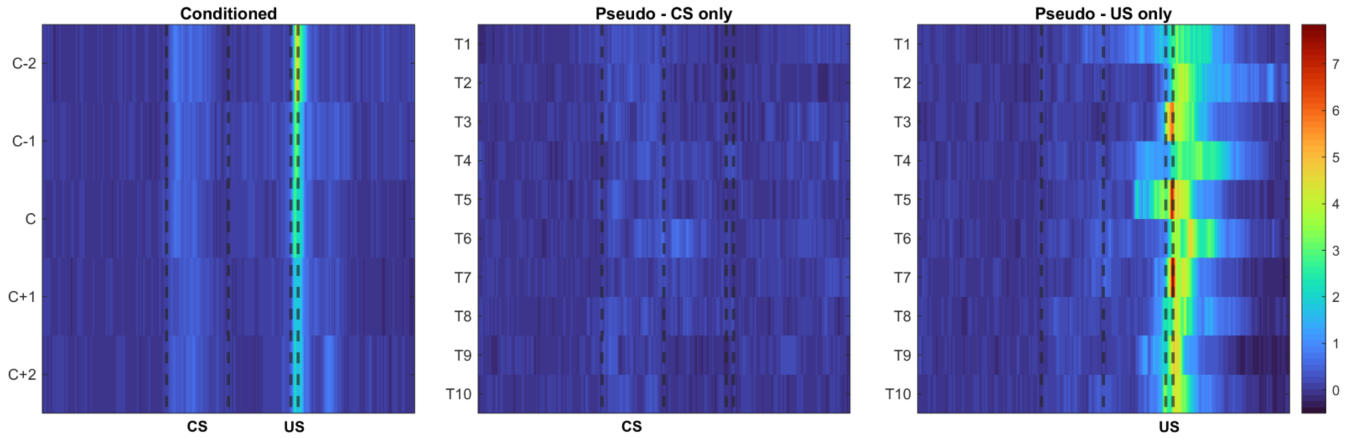

FIGURE 9 Theta power in DG during training. Conditioned animals ($n = 9$) show a significant increase in theta power during CS and US presentation (CS: $F[1, 12] = 18.35$, $p = .0011$; US: $F[1, 12] = 5.40$, $p = .039$) that decreases from pre-criterion to post-criterion (CS: $F[4, 48] = 3.16$, $p = .022$; US: $F[4, 48] = 2.95$, $p = .029$). Pseudoconditioned animals ($n = 5$) show a large increase in theta power during US presentation ($F[1, 8] = 21.15$, $p = .0018$), but no significant change in theta power during CS presentation ($F[1, 8] = 3.28$, $p = .11$). Each row represents a different day, where "C" refers to the day of criterion for conditioned mice and "T" refers to day of training for pseudo mice. CS, conditioned stimulus; DG, dentate gyrus; US, unconditioned stimulus

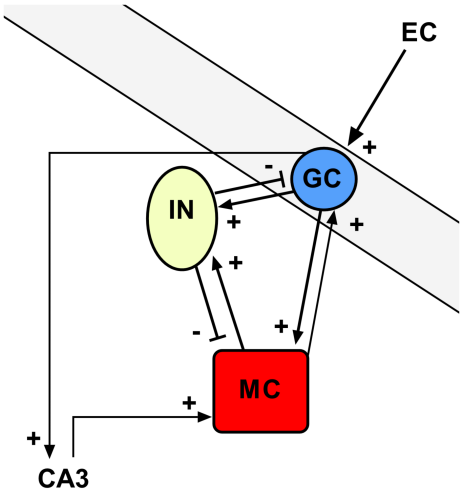

FIGURE 10 Simplified DG circuitry. In conditioned mice, stimulus information is passed to granule cells from entorhinal cortex. Increased GC activity leads to direct excitation of INs, and after repeated stimulation, wINs show persistent firing that spans the trace interval. This persistent activity leads to a direct decrease in MC activity during the trace and US intervals due to the increased inhibitory inputs. Decreased MC activity should decrease the excitatory drive arriving at INs, which would reduce the inhibitory drive on GCs, ultimately promoting GC activity. Finally, GCs send processed information to the CA3 region of the hippocampus. In this diagram, "IN" represents both wINs and nINs. CS, conditioned stimulus; DG, dentate gyrus; GC, granule cell; IN, interneuron; MC, mossy cell; nIN, narrow-waveform interneuron; US, unconditioned stimulus; wIN, wide-waveform interneuron

from DG INs to refine this response pattern. Additionally, pyramidal cells recorded from CA1 during tEBC show various response patterns, including an increase or decrease in activity that spans the trace interval (Hattori et al., 2014; McEchron & Disterhoft, 1997; Weible et al., 2006). Inhibition from DG could influence these response patterns, and the increased CA1 activity could support temporal learning by bridging the gap between stimuli.

Both male and female mice were used in the current study, and we observed that while both sexes successfully learned, male mice with the microdrive implant learned at a faster rate than female mice. While past studies have demonstrated that female animals learn tEBC faster than male animals (Dalla et al., 2009; Rapp, Weiss, et al., 2021), our findings are in accordance with work that describes the effects of chronic microdrive implantation on associative learning (Rapp, Hark, et al., 2022). In Rapp, Hark, et al. (2022), male mice with microdrive implants learned tEBC faster than female microdrive mice, and it was hypothesized that this sexually dimorphic behavior was due to the neuroinflammatory response caused by the craniotomy and tetrode implantation. The current study shows the same trends in learning as this previous study, although more work is necessary to confirm whether these sex differences can be fully attributed to neuroinflammation.

The current study has some limitations, such as the low number of neurons recorded from DG. While there were no apparent differences in cellular responses between male and female mice, a larger number of neurons would be necessary to definitively draw a conclusion regarding sex differences. Similarly, more neurons from each day of training would be necessary to make conclusions about how the changes in cellular activity relate to behavioral expression of learning (e.g., pre-criterion vs. post-criterion). Additionally, while we were able to separate putative INs into two groups based on their firing properties, we are unable to confirm the identities of these INs any further. Based solely on their firing properties, we could hypothesize that the nINs we recorded from are parvalbumin-expressing INs, while the wINs are somatostatin-expressing INs. However, one would need to use juxtacellular recording, optogenetics, or in vivo calcium imaging in order to accurately determine which subpopulations of INs underlie the learning-related changes observed in these data, as well as definitively confirm the identities of GCs and MCs. Additionally, recording during

sleep or open field testing (to determine the number of place fields) would provide additional information that would be useful in distinguishing between GCs and MCs based on physiological properties alone (GoodSmith et al., 2017; Neunuebel & Knierim, 2012, 2014; Senzai & Buzsáki, 2017). Other useful approaches for differentiating cell types in future studies may be examining gamma coupling of single units or determining the spike autocorrelogram refractory gap for each cell (Jung et al., 2019; Kim et al., 2020).

Drew et al. (2015) demonstrated that optogenetic stimulation of adult-born neurons activates INs to evoke inhibitory input to mature GCs, and that stimulation of these immature neurons in vivo reduced the number of GCs activated by exploration. These data suggest a role for adult neurogenesis in modulating INs to influence GC activity. Additionally, Kheirbek et al. (2013) used optogenetic inhibition and excitation of GCs to demonstrate the importance of dorsal GCs in learning and ventral GCs in anxiety. Both of these studies show that optogenetics is a powerful tool to investigate the DG circuit and determine how DG cell types influence behavior.

Ultimately, the current study demonstrates clear learning-related changes in GCs, MCs, and INs within DG during an associative learning task. Specifically, GCs seem to carry stimulus information, while INs undergo enhanced excitability over time, which may help refine distinct neural connections during memory formation. While tEBC is not a direct test of pattern separation, it is possible the task could still involve pattern separation, as task performance requires the ability to discriminate between the CS and other stimuli that were not specifically presented during training (i.e., contextual stimuli in the environment surrounding the mice during training). Regardless, these findings demonstrate unique activity patterns in DG cell types during hippocampal-dependent, temporal associative learning. While further work is necessary to understand how these changes in activity develop over the course of learning, these data provide a base of knowledge on how DG contributes to associative learning at the circuit level.

ACKNOWLEDGMENTS

The authors would like to thank Venus Sherathiya, Dr. Hannah Wirtshafter, and Dr. Amy Rapp for their technical support and valuable feedback.

FUNDING INFORMATION

This works was supported by the NIH through grants RF1 AG017139 and R37 AG008796 to John F. Disterhoft.

CONFLICT OF INTEREST

None of the authors have any competing interests to declare.

DATA AVAILABILITY STATEMENT

The data that support the findings of this study are available from the corresponding author upon reasonable request.

ORCID

Lisa N. Miller https://orcid.org/0000-0001-7677-6604
Craig Weiss https://orcid.org/0000-0002-9861-8727
John F. Disterhoft https://orcid.org/0000-0002-8817-7913

REFERENCES

Amaral, D. G. (1978). A Golgi study of cell types in the hilar region of the hippocampus in the rat. *Journal of Comparative Neurology*, *182*, 851–914. https://doi.org/10.1002/cne.901820508

Amaral, D. G., Ishizuka, N., & Claiborne, B. (1990). Neurons, numbers and the hippocampal network. *Progress in Brain Research*, *83*, 1–11. https://doi.org/10.1016/S0079-6123(08)61237-6

Andrews-Zwilling, Y., Gillespie, A. K., Kravitz, A. V., Nelson, A. B., Devidze, N., Lo, I., Yoon, S. Y., Bien-Ly, N., Ring, K., Zwilling, D., Potter, G. B., Rubenstein, J. L. R., Kreitzer, A. C., & Huang, Y. (2012). Hilar GABAergic interneuron activity controls spatial learning and memory retrieval. *PLoS One*, *7*(7), e40555. https://doi.org/10.1371/journal.pone.0040555

Berger, T. W., Alger, B., & Thompson, R. F. (1976). Neuronal substrate of classical conditioning in the hippocampus. *Science*, *192*(4238), 483–485. https://doi.org/10.1126/science.1257783

Berger, T. W., & Thompson, R. F. (1978). Neuronal plasticity in the limbic syste during classical conditioning of the rabbit nictitating membrane response II: Septum and mammillary bodies. *Brain Research*, *156*(2), 293–314. https://doi.org/10.1016/0006-8993(78)90510-3

Bernier, B., Lacagnina, A., Ayoub, A., Shue, F., Zemelman, B., Krasne, F., & Drew, M. (2017). Dentate gyrus contributes to retrieval as well as encoding: Evidence from context fear conditioning, recall, and extinction. *Journal of Neuroscience*, *37*(26), 6359–6371. https://doi.org/10.1523/JNEUROSCI.3029-16.2017

Botterill, J. J., Vinod, K. Y., Gerencer, K. J., Teixeira, C. M., LaFrancois, J. J., & Scharfman, H. E. (2021). Bidirectional regulation of cognitive and anxiety-like behaviors by dentate gyrus mossy cells in male and female mice. *Journal of Neuroscience*, *41*(11), 2475–2495. https://doi.org/10.1523/JNEUROSCI.1724-20.2021

Bragin, A., Jando, G., Nadasdy, Z., Van Landeghem, M., & Buzsáki, G. (1995). Dentate EEG spikes and associated interneuronal population bursts in the hippocampal hilar region of the rat. *Journal of Neurophysiology*, *73*(4), 1691–1705. https://doi.org/10.1152/jn.1995.73.4.1691

Buckmaster, P. S., Yamawaki, R., & Zhang, G. F. (2002). Axon arbors and synaptic connections of a vulnerable population of interneurons in the dentate gyrus in vivo. *Journal of Comparative Neurology*, *445*, 360–373. https://doi.org/10.1002/cne.10183

Bui, A. D., Nguyen, T. M., Limouse, C., Kim, H. K., Szabo, G. G., Felong, S., Maroso, M., & Soltesz, I. (2018). Dentate gyrus mossy cells control spontaneous convulsive seizures and spatial memory. *Science*, *359*(6377), 787–790. https://doi.org/10.1126/science.aan4074

Chen, S., Chen, F., Amin, N., Ren, Q., Ye, S., Hu, Z., Tan, X., Jiang, M., & Fang, M. (2021). Defects of parvalbumin-positive interneurons in the ventral dentate gyrus region are implicated depression-like behavior in mice. *Brain, Behavior, and Immunity*, *99*, 27–42. https://doi.org/10.1016/j.bbi.2021.09.013

Chi, V. N., Müller, C., Wolfenstetter, T., Yanovsky, Y., Draguhn, A., Tort, A. B. L., & Brankačk, J. (2016). Hippocampal respiration-driven rhythm distinct from theta oscillations in awake mice. *Journal of Neuroscience*, *36*(1), 162–177. https://doi.org/10.1523/JNEUROSCI.2848-15.2016

Chung, J. E., Magland, J. F., Barnett, A. H., Tolosa, V. M., Tooker, A. C., Lee, K. Y., Shah, K. G., Felix, S. H., Frank, L. M., & Greengard, L. F. (2017). A fully automated approach to spike sorting. *Neuron*, *95*(6), 1381–1394. https://doi.org/10.1016/j.neuron.2017.08.030

Dalla, C., Papachristos, E. B., Whetstone, A. S., & Shors, T. J. (2009). Female rats learn trace memories better than male rats and consequently retain a greater proportion of new neurons in their hippocampi. *Proceedings of the National Academy of Sciences of the United States of America*, *106*(8), 2927–2932. https://doi.org/10.1073/pnas.0809650106

Drew, L. J., Kheirbek, M. A., Luna, V. M., Denny, C. A., Cloidt, M. A., Wu, M. V., Jain, S., Scharfman, H. E., & Hen, R. (2015). Activation of local inhibitory circuits in the dentate gyrus by adult-born neurons. *Hippocampus*, *26*(6), 763–778. https://doi.org/10.1002/hipo.22557

Elgueta, C., Köhler, J., & Bartos, M. (2015). Persistent discharges in dentate gyrus perisoma-inhibiting interneurons require hyperpolarization-activated

cyclic nucleotide-gated channel activation. *Journal of Neuroscience*, *35*(10), 4131–4139. https://doi.org/10.1523/JNEUROSCI.3671-14.2015

Fritz, A. K., Amrein, I., & Wolfer, D. P. (2017). Similar reliability and equivalent performance of female and male mice in the open field and water-maze place navigation task. *American Journal of Medical Genetics*, *175*(3), 380–391. https://doi.org/10.1002/ajmg.c.31565

Gilmartin, M. R., & McEchron, M. D. (2005). Single neurons in the dentate gyrus and CA1 of the hippocampus exhibit inverse patterns of encoding during trace fear conditioning. *Behavioral Neuroscience*, *119*(1), 164–179. https://doi.org/10.1037/0735-7044.119.1.164

GoodSmith, D., Chen, X., Wang, C., Kim, S. H., Song, H., Burgalossi, A., Christian, K. M., & Knierim, J. J. (2017). Spatial representations of granule cells and mossy cells of the dentate gyrus. *Neuron*, *93*(3), 677–690. https://doi.org/10.1016/j.neuron.2016.12.026

GoodSmith, D., Kim, S. H., Puliyadi, V., Ming, G. L., Song, H., Knierim, J. J., & Christian, K. M. (2022). Flexible encoding of objects and space in single cells of the dentate gyrus. *Current Biology*, *32*, 1088–1101. https://doi.org/10.1016/j.cub.2022.01.023

Hainmueller, T., & Bartos, M. (2020). Dentate gyrus circuits for encoding, retrieval, and discrimination of episodic memories. *Nature Reviews Neuroscience*, *21*(3), 153–168. https://doi.org/10.1038/s41583-019-0260-z

Hattori, S., Chen, L., Weiss, C., & Disterhoft, J. F. (2014). Robust hippocampal responsivity during retrieval of consolidated associative memory. *Hippocampus*, *25*(5), 655–669. https://doi.org/10.1002/hipo.22401

Heiney, S. A., Wohl, M. P., Chettih, S. N., Ruffolo, L. I., & Medina, J. F. (2014). Cerebellar-dependent expression of motor learning during eyeblink conditioning in head-fixed mice. *Journal of Neuroscience*, *34*(45), 14845–14853. https://doi.org/10.1523/JNEUROSCI.2820-14.2014

Henze, D. A., & Buzsáki, G. (2007). Hilar mossy cells: Functional identification and activity in vivo. *Progress in Brain Research*, *163*, 199–216. https://doi.org/10.1016/S0079-6123(07)63012-X

Jinde, S., Zsiros, V., Jiang, Z., Nakao, K., Pickel, J., Kohno, K., Belforte, J., & Nakazawa, K. (2012). Hilar mossy cell degeneration causes transient dentate granule cell Hyperexcitability and impaired pattern separation. *Neuron*, *76*(6), 1189–1200. https://doi.org/10.1016/j.neuron.2012.10.036

Jinde, S., Zsiros, V., & Nakazawa, K. (2013). Hilar mossy cell circuitry controlling dentate granule cell excitability. *Frontiers in Neural Circuits*, *7*, 14. https://doi.org/10.3389/fncir.2013.00014

Jung, D., Kim, S., Sariev, A., Sharif, F., Kim, D., & Royer, S. (2019). Dentate granule and mossy cells exhibit distinct spatiotemporal responses to local change in a one-dimensional landscape of visual-tactile cues. *Scientific Reports*, *9*, 9545. https://doi.org/10.1038/s41598-019-45983-6

Kheirbek, M., Drew, L., Burghardt, N., Costantini, D., Tannenholz, L., Ahmari, S., Zeng, H., Fenton, A., & Hen, R. (2013). Differential control of learning and anxiety along the dorso-ventral axis of the dentate gyrus. *Neuron*, *77*(5), 955–968. https://doi.org/10.1016/j.neuron.2012.12.038

Kim, S., Jung, D., & Royer, S. (2020). Place cell maps slowly develop via competitive learning and conjunctive coding in the dentate gyrus. *Nature Communications*, *11*, 4550. https://doi.org/10.1038/s41467-020-18351-6

Kitamura, T., Sun, C., Martin, J., Kitch, L. J., Schnitzer, M. J., & Tonegawa, S. (2015). Entorhinal cortical ocean cells encode specific contexts and drive context-specific fear memory. *Neuron*, *87*(6), 1317–1331. https://doi.org/10.1016/j.neuron.2015.08.036

Lee, C. T., Kao, M. H., Hou, W. H., Wei, Y. T., Chen, C. L., & Lien, C. C. (2016). Causal evidence for the role of specific GABAergic interneuron types in entorhinal recruitment of dentate granule cells. *Scientific Reports*, *6*, 36885. https://doi.org/10.1038/srep36885

Lin, C., Disterhoft, J., & Weiss, C. (2016). Whisker-signaled eyeblink classical conditioning in head-fixed mice. *Journal of Visualized Experiments*, *109*, e53310. https://doi.org/10.3791/53310

McEchron, M. D., & Disterhoft, J. F. (1997). Sequence of single neuron changes in CA1 hippocampus of rabbits during acquisition of trace eyeblink conditioned responses. *Journal of Neurophysiology*, *78*(2), 1030–1044. https://doi.org/10.1152/jn.1997.78.2.1030

McKay, B. M., Oh, M. M., & Disterhoft, J. F. (2013). Learning increases intrinsic excitability of hippocampal interneurons. *Journal of Neuroscience*, *33*(13), 5499–5506. https://doi.org/10.1523/JNEUROSCI.4068-12.2013

Neunuebel, J. P., & Knierim, J. J. (2012). Spatial firing correlates of physiologically distinct cell types of the rat dentate gyrus. *Journal of Neuroscience*, *32*(11), 3848–3858. https://doi.org/10.1523/JNEUROSCI.6038-11.2012

Neunuebel, J. P., & Knierim, J. J. (2014). CA3 retrieves coherent representations from degraded input: Direct evidence for CA3 pattern completion and dentate gyrus pattern separation. *Neuron*, *81*, 416–427. https://doi.org/10.1016/j.neuron.2013.11.017

Pierson, J. L., Pullins, S. E., & Quinn, J. J. (2015). Dorsal hippocampus infusions of CNQX into the dentate gyrus disrupt expression of trace fear conditioning. *Hippocampus*, *25*, 779–785. https://doi.org/10.1002/hipo.22413

Prendergast, B. J., Onishi, K. G., & Zucker, I. (2014). Female mice liberated for inclusion in neuroscience and biomedical research. *Neuroscience & Biobehavioral Reviews*, *40*, 1–5. https://doi.org/10.1016/j.neubiorev.2014.01.001

Rapp, A. P., Weiss, C., Oh, M. M., & Disterhoft, J. F. (2021). Intact female mice acquire trace eyeblink conditioning faster than male and ovariectomized female mice. *eNeuro*, *8*(2), ENEURO.0199–ENEU20.2021. https://doi.org/10.1523/ENEURO.0199-20.2021

Rapp, A. P., Hark, T. J., Power, J. M., Savas, J. N., Oh, M. M., & Disterhoft, J. F. (2022). Sex-dependent effects of chronic microdrive implantation on acquisition of trace eyeblink conditioning. *Neurobiology of Learning and Memory*, *193*, 107649. https://doi.org/10.1016/j.nlm.2022.107649

Royer, S., Zemelman, B. V., Losonczy, A., Kim, J., Chance, F., Magee, J. C., & Buzsáki, G. (2012). Control of timing, rate and bursts of hippocampal place cells by dendritic and somatic inhibition. *Nature Neuroscience*, *15*(5), 769–779. https://doi.org/10.1038/nn.3077

Savanthrapadian, S., Meyer, T., Elgueta, C., Booker, S. A., Vida, I., & Bartos, M. (2014). Synaptic properties of SOM- and CCK-expressing cells in dentate gyrus interneuron networks. *Journal of Neuroscience*, *34*(24), 8197–8209. https://doi.org/10.1523/JNEUROSCI.5433-13.2014

Senzai, Y., & Buzsáki, G. (2017). Physiological properties and behavioral correlates of hippocampal granule cells and mossy cells. *Neuron*, *93*(3), 691–704. https://doi.org/10.1016/j.neuron.2016.12.011

Suter, E. E., Weiss, C., & Disterhoft, J. F. (2018). Differential responsivity of neurons in perirhinal cortex, lateral entorhinal cortex, and dentate gyrus during time-bridging learning. *Hippocampus*, *29*(6), 511–526. https://doi.org/10.1002/hipo.23041

Weible, A. P., O'Reilly, J. A., Weiss, C., & Disterhoft, J. F. (2006). Comparisons of dorsal and ventral hippocampus cornu ammonis region 1 pyramidal neuron activity during trace eyeblink conditioning in the rabbit. *Neuroscience*, *141*(3), 1123–1137. https://doi.org/10.1016/j.neuroscience.2006.04.065

Yassa, M. A., & Stark, C. E. L. (2011). Pattern separation in the hippocampus. *Trends in Neuroscience*, *34*, 515–525. https://doi.org/10.1016/j.tins.2011.06.006

Yu, X., Yu, J., Choi, A., & Takehara-Nishiuchi, K. (2021). Lateral entorhinal cortex supports the development of prefrontal network activity that bridges temporally discontiguous stimuli. *Hippocampus*, *31*(12), 1285–1299. https://doi.org/10.1002/hipo.23389

Yuan, M., Meyer, T., Benkowitz, C., Savanthrapadian, S., Ansel-Bollepalli, L., Foggetti, A., Wulff, P., Alcami, P., Elgueta, C., & Bartos, M. (2017). Somatostatin-positive interneurons in the dentate gyrus of mice provide local- and long-range septal synaptic inhibition. *eLife*, *6*, e21105. https://doi.org/10.7554/eLife.21105

How to cite this article: Miller, L. N., Weiss, C., & Disterhoft, J. F. (2022). Learning-related changes in cellular activity within mouse dentate gyrus during trace eyeblink conditioning. *Hippocampus*, *32*(10), 776–794. https://doi.org/10.1002/hipo.23468